On the Anatomy of Acoustic Emission

Robert A. Guyer[1,2], **Samson Marty**[3], **Chris Marone**[4], **Paul A. Johnson**[2], **Christopher W. Johnson**[2]

[1]Physics, University of Nevada-Reno, NV, USA
[2]Los Alamos National Laboratory, Los Alamos, NM, USA
[3]California Institute of Technology, Pasadena, CA, USA
[4]Sapienza University, Rome, Italy

Key Points:

- A properly formulated measure of the acoustic emission is introduced to define *white* (disposable) and *articulate* (informational) components.
- The acoustic emission *articulate* component describes the slider displacement in laboratory earthquake shear experiments.
- The acoustic emission *articulate* component explains mapping to fault mechanical properties.

Corresponding author: C. W. Johnson, `cwj@lanl.gov`

Abstract

Abrupt frictional fault failure is normally accompanied by acoustic emission (AE)—impulsive elastic wave broadcast—with amplitude proportional to particle velocity. The cumulative sum of the fault particle velocities is a slip displacement. In laboratory shear experiments described here, measurements of a sequence of laboratory earthquakes includes local measurement of fault displacement and AE. Using these measurements we illuminate the connections between "cumulative sum of AE" and "slip displacement". Additionally, the composition of the AE broadcasts reveals inhomogeneity in the fault mechanical structure from which they arise. This inhomogeneity, leading to a time invariant *white* AE component and an *articulated* AE, indicates that the *articulated* cumulative sum of the AE reveals a fault "state of the mechanical structure" diagnostic, that follows a distinctive pattern to frictional failure. This pattern explains why the continuous AE map to fault displacement as well as fault friction, shear stress, etc., as shown in many recent studies.

Plain English

In two hundred and fifty BCE Archimedes measured the volume of an oddly shaped object by slowly lowering it into a filled glass of water and determining the spillage. The motion in an inaccessible, seismically active zone is coded in the "spillage" of elastic waves from the active zones interior. Today 2024 CE Archimedes can listen to the spillage of elastic waves and deduce the active zones motion. This 2024 CE principle is stated and confirmed in this paper.

1 Introduction

In the last decade it has been discovered that continuous dynamic elastic wave broadcasts from laboratory faults, referred to here as acoustic emission (AE), are rich with information beyond classical precursors to frictional failure (P. A. Johnson et al., 2021, and references therein). By applying machine learning models to the continuous waveforms, these AEs can show where the fault is in the slip cycle. With this demonstration, a fundamental open question is why. The AE from a seismic zone carry an evolving record throughout the earthquake cycle describing the fault zone mechanics that presage the next "big" event. This observation helps drive the extant enthusiasm for the value of new powerful machine-learning-based data acquisition and analysis schemes being used in studying seismology problems (Bergen et al., 2019; Mousavi & Beroza, 2022, 2023).

Today there are an abundance of high-fidelity AE data and state-of-the-art data processing techniques driving these new analyses (Beroza et al., 2021; Kong et al., 2018). One example of current practice, and the focus here, is the successful use of machine learning methods to glean seismic zone evolution from the temporally evolving feature space of the continuous AE (C. W. Johnson et al., 2020; Lubbers et al., 2018; C. W. Johnson & Johnson, 2023; Rouet-Leduc et al., 2019b, 2017; Hulbert et al., 2019, 2020; Corbi et al., 2019; Shreedharan et al., 2021; Rouet-Leduc et al., 2019a; Wang et al., 2021, 2022; Borate et al., 2023; Seydoux et al., 2020; Holtzman et al., 2018; Jasperson et al., 2021; Shokouhi et al., 2021; Laurenti et al., 2022). In this study, we step back from the current machine learning practice to understand why the AE is a powerful predictor of contemporaneous displacement, friction, etc. We do so by analyzing data from a carefully instrumented laboratory bi-axial "earthquake machine" experiment. The experiment analyzed (p5702) is typical of those conducted on a double direct shear device (e.g., Bolton et al., 2021) and allows us to follow the AE while the mechanical state of the "earthquake machine" unfolds. Thus, we can decompose the AE into separable components that have understandable behavior and understandable participation in the evolution of the mechanical state.

2 Laboratory Data

2.1 p5702 Earthquake Experiment

The experiment comprises a granite slider block that is pushed between two granite substrate blocks by a normal stress (N) of $6, 9, 12, 15$ MPa respectively, during the experiment. See Supporting Information Figure S1a for a schematic of the system and complete details. The granite slider block is driven at a constant servo-controlled load point velocity of $V_0 = 10$ $\mu m/sec$. The slider-substrate interfacial region (yellow area shown in Figure S1a) comprises a shear support structure that carries the shear stress between slider and substrate. Broadcasts from this region are the AE as the shear support structure evolves in time through asperity and fault gouge breaking, rearranging, resetting, etc. and typically detected away from the interfacial region. The experiment is designed so that the normal stress (N) is applied uniformly over a 100 cm^2 area, but it passes non-uniformly through this area due to the shear support structure (e.g., Latour et al., 2013; Selvadurai & Glaser, 2016; Caniven et al., 2017).

The state of the mechanical system is set by the choice of normal stress and load point velocity (N, V_0). Measurements are made through time of (1) the shear stress (determined from the applied stress in the load cell), (2) the position of the on-board-displacement point (relative to the two side blocks in the laboratory frame of reference), and (3) the AE (15-bit Verasonics data acquisition system continuously recording at 4 MHz using broadband ∼0.0001–2 MHz piezoceramic sensors and downsampled to 100 kHz). Under the conditions (N, V_0) for the p5702 experiment, the motion of the slider undergoes repeated slip-stick cycles of approximately constant duration as observed in the shear stress through time (Figure S1b). The length of substrate crossed in a slip-stick cycle is of order $50-100$ μm (dependent on N). For example at $N = 6$ MPa, during slip the slider moves quickly (0.4 seconds) through about 40 μm followed by "creep" for about 5 seconds through an additional 7 μm. During creep the composition of the AE evolves as the slip-stick cycle unfolds. This evolution of the AE is a target of our investigation.

2.2 Displacement

To track the motion of the slider we examine the on-board-displacement, denoted X_S, that locates the slider block relative to the laboratory reference frame. In Figure 1a we show X_S through time for the last six slip-stick events at $N = 6$ MPa. Note, there is a slow evolution of the amplitude of the slip-stick behavior throughout the experiment as shown in Figure S1b and described in the Supporting Information. To minimize the effect of this evolution, we examine the last six slip-stick events at each applied normal stress (N). These six events are part of a set of steps; there is a "riser" shown by an increase in X_S of about 40 μm that is abrupt in time and a "tread" having complex behavior as seen in the Figure 1b. To describe X_S on the "tread", we fit X_S to a line of constant slope, $X_S = Ut + h$, where h allows us to align the "treads". For the six "treads" in Figure 1, the slopes U are 0.0014, 0.0013, 0.0013, 0.0013, 0.0013, 0.0012 mm/sec; very consistent among themselves with U about 10% of the load point velocity, $V_0 = 0.01$ mm/sec. At no point on the "tread" is $dX_S/dt = 0$. We further decompose X_S by examining the difference between the X_S on the "tread" and the model Ut. We show $X_S - Ut$, the residual, in Figure 2. The residual is typically of order 0.001 mm and less than $UT_{SS} \approx 0.007$ mm, where T_{SS} is the time on "tread" (see Table S1 in the Supporting Information for numerical details). The residual is *articulated* in time, i.e., it varies in time markedly over the "tread" in much the same way for all six slip-stick events.

We adopt the view that the slider-interface is inhomogeneous with some regions at essentially constant friction that are sliding parallel to other regions containing shear support structures with sufficient strength to deliver a noticeable impulse to the slider. Thus, the displacement X_S on the "tread" comprise two components; a *white* component (going as Ut) and a *articulated* component (varying non-trivially in time) as the slider crosses the "tread". This articulated component of X_S is shown in Figure 2.

2.3 Acoustic Emission (AE)

We inform our treatment of the AE by the mechanical perspective described above. There are important prefacing remarks gleaned from numerical experiments (Gao et al., 2018, 2019, 2020), as follows. When an element of the shear support structure fails, a short lived force dipole, with strength δF, appears in the system. One component of the dipole pushes the slider toward the load point and the other component pushes the (massive) substrate backward. An elastic wave is launched from the domain of the failure and a velocity impulse δv is delivered to the slider proportional to the strength δF of the failed support structure. Additionally, the elastic wave, which is a contribution to the AE, is broadcast with an amplitude that is proportional to $\delta F \propto \delta v$. All δF and δv are positive since a failure pushes the slider toward the load point. The expectation is that the integral over time of the *magnitude* of the AE, approximately an integral over δv, is proportional to the displacement of the slider. Instead of studying the raw AE, we study the AE in the context of this expectation, i.e., we study

$$\mathcal{C}(t) = \int_0^t \beta(t^{'})\, dt^{'}, \quad 0 \leq t \;\; on \;\; the \;\; \text{"}tread\text{"}, \tag{1}$$

where $\beta(t)$ is the upper envelope of the AE, $\alpha(t)$, detected at time t.

In Figure S2a we show the $N = 6\ MPa$ AE $\alpha(t)$ for one "tread" where the adjacent slider block slips are at the bounding red lines. The "tread" is about 5 seconds in duration and is sampled by about 5×10^5 data points. In Figure S2b we show $\beta(t)$, the upper envelope of $\alpha(t)$. In Figure 3 we show $\mathcal{C}(t)$ vs t from Equation 1 for six slip-stick events during each of the four applied normal stresses N. The quantity shown is $\mathcal{C}(t)$ on each "tread" divided by the length of time of the "tread" to scale $\mathcal{C}(t)$ so the results fit conveniently on a single plot.

The striking feature of the behavior of $\mathcal{C}(t)$ is that in leading approximation, for all six slip-stick events and for all four applied normal stresses N, $\mathcal{C}(t)$ rises linearly with time. That is, $\beta(t)$ is essentially constant through time, $\int_0^t \beta(t)dt \approx \beta \int_0^t dt$. This may not be apparent when looking at the continuous s (Figure S2b). The noticeable spikes in $\beta(t)$ are weighted by their time duration in the construction of $\mathcal{C}(t)$ and are minimally contributing amidst the large number of nearly continuous smaller amplitude contributions. Emulating the treatment of the on-board-displacement we fit $\mathcal{C}(t)$ to a line: $\mathcal{C}(t) = Wt$. Then, in Figure 4 we show the residual, $\mathcal{C}(t){-}Wt$, for the six "treads" during the four applied normal stresses N. We note that the residual is essentially the same for each of the six "treads" for each applied normal stresses N. The shape in time of the residual is much the same for all N. The residual, $\mathcal{C}(t) - Wt$, closely resembles the articulate component of the on-board-displacement, Figure 2. These findings support the assertion, based on the "prefacing remarks", of the physical connection between the construct involving the AE, Equation 1, and the on-board-displacement.

3 Results and Discussion

The data show both X_S and $\mathcal{C}(t)$ on a "tread" comprise a *white* component that is trivially dependent on t, with no important structure in time beyond proportionality (Figure 3). By removing the *white* component to isolate the *articulated* component it becomes evident there is structure in time to X_S and to $\mathcal{C}(t)$ over the entire length of the "tread" (Figures 2 and 4). The similarity of the *articulated* component of X_S and the *articulated* component of $\mathcal{C}$ demonstrate the connection between the load-point-displacement X_S and AE $\alpha(t)$ that informed our data treatment. The two parts of X_S and $\mathcal{C}(t)$ belong to the two parts of the inhomogeneous shear support structure. They exist adjacent to one another (Trugman et al., 2020) and are associated with two different friction components. An equation of motion for the slider might take the form

$$M\ddot{X} = k(V_0 t - X) - F_w - F_a, \tag{2}$$

where F_w and F_a are the forces associated with the *white* and *articulated* components. The spatial domains of the two components of the shear support structure are determined by the way in which the normal stress crosses through the shear support structure. These spatial domains appear to be approximately "location invariant", i.e., they retain their integrity as the slider goes through repeated slip-stick cycles as seen in Trugman et al. (2020) and Marty et al. (2023).

In Table S1 we show the numerical values of the parameter that describe the motion of the slider over one slip-stick cycle length. During slip the *articulated* component of the shear support structure is dis-engaged and the slider rapidly advances distance b_0 (ranging from 37 μm to 151 μm as N increases). Slip stops abruptly when the *articulated* component of the shear support structure re-engages, holding the slider to approximately constant velocity (from ≈ 1 $\mu m/sec$ to ≈ 0.2 $\mu m/sec$ as N increases), then slow motion toward a new slip unfolds. The slip-to-slip time, T_{SS}, basically the time on the "tread", varies from 5.5 sec to 22.6 sec as the applied normal stress N increases. Both b_0 and T_{SS} scale approximately with N. The total slip-stick length, $b_0{+}UT_{ss}$, varies from 44 μm to 155 μm as N increases.

In Table S2 we show the numerical values of the parameters that describe the cumulative AE over one slip-stick length. The cumulative AE, $\mathcal{C}(t)$ varies from 24.54 to 105.07 as N increases. It comprises a *white* component, which is almost all of it, and the *articulated* component shown in Figure 4. The *articulated* component of $\mathcal{C}(t)$ is of order 1% of the total (listed in the last column of Table S2). Interestingly, the velocity W with which $\mathcal{C}(t)$ increases on a "tread" is approximately independent of the applied normal stress N. In Table S3 we list the independent scaling with N of the parameters describing the behavior of X_S and $\mathcal{C}$.

4 Conclusions

We have undertaken the study of a laboratory earthquake system for which we have access to measurement of (1) the on-board-displacement, X_S, and (2) the AE, $\alpha(t)$. Therefore, we can conduct an empirical test of the relationship between mechanical variables (displacement, stress, ...) and the AE. Our treatment of the analysis is informed by a physical model of shear support structure (Gao et al., 2019) to form $\mathcal{C}$, the cumulative sum of the magnitude of the AE. Both X_S and $\mathcal{C}$ are able to be separated into a *white* component and an *articulated* component. For both X_S and $\mathcal{C}$ the *white* component is time independent as the system moves between slip events. In contrast, the *articulated* component of $\mathcal{C}$ and $\mathcal{C}_a$, has much the same time dependence as the *articulated* component of X_S and X_a. This similarity is present during repeated stick domains (i.e., between slip events) for each normal stress as it is varied from 6 MPa to 15 MPa (Figure 2). We take these similarities to establish that $\mathcal{C}_a$ is essentially equivalent to the articulated part of X_S. That is, the important motion of the slider in time, $X_a(t)$, can be tracked by following a properly formed (i.e., Gao et al., 2019) measure of the AE, i.e., $\mathcal{C}_a(t)$. From 2024 CE "Archimedes" (Plain English) $\mathcal{C}_a(t)$ is a valid diagnostic for following slider motion through time. [There are important differences in Figures 2 and 4 early in time. These differences arise because the timing on a "tread" in the mechanical data is set by the on-board-displacement "jump", whereas, the timing in the AE data is set by the "noise pulse" in that data.]

How are the findings here related to the recent studies employing AE? In the typical machine learning based AE study (e.g., Rouet-Leduc et al., 2017) the basic outcome is a point-wise in time equation of state, i.e., at each moment of time a one-to-one correspondence is established between the properties of the feature space derived from the AE and the shear stress state of the slider. It is straight forward in such calculations to replace the shear stress state of the slider with the on-board displacement. Then, an equation of state, that is at each time a one-to-one correspondence between the properties of the feature space of the AE and the on-board-displacement, can be established. In short, the machine learning model is applied in these calculations in order to find within the AE the set of features that carry the information correlated with the on board displacement. For instance, in laboratory shear experiments (Rouet-Leduc et al., 2017) a single feature equation of state is demonstrated from laboratory experiment AEs and in repeating caldera collapse sequence (C. W. Johnson & Johnson, 2023) an equation of state is demonstrated using AEs that carry the evolving ground displacement information. That is why the machine learning analyses "work" and similarities in the *articulated* components emphasizes this point.

Data Availability Statement

Data used in this study are publicly available at https//doi.org/10.26207/rcgg-x946.

Acknowledgments

This material is based upon work supported by the U.S. Department of Energy, Office of Science, Office of Basic Energy Sciences, Geosciences program under Award Number DE-FG02-09ER16022.

References

Bergen, K. J., Johnson, P. A., de Hoop, M. V., & Beroza, G. C. (2019). Machine learning for data-driven discovery in solid earth geoscience. *Science*, *363*(6433), eaau0323. Retrieved from `https://www.science.org/doi/abs/10.1126/science.aau0323` doi: 10.1126/science.aau0323

Beroza, G., Segou, M., & Mousavi, S. (2021, 12). Machine learning and earthquake forecasting—next steps. *Nature Communications*, *12*. doi: 10.1038/s41467-021-24952-6

Bolton, D., Shreedharan, S., Riviere, J., & Marone, C. (2021). Frequency magnitude statistics of laboratory foreshocks. *JGR Solid Earth.*, *126*, e2021JB022175.

Borate, P., Rivière, J., Marone, C., Mali, A., Kifer, D., & Shokouhi, P. (2023, 06). Using a physics-informed neural network and fault zone acoustic monitoring to predict lab earthquakes. *Nature Communications*, *14*. doi: 10.1038/s41467-023-39377-6

Caniven, Y., Dominguez, S., Soliva, R., Peyret, M., Cattin, R., & Maerten, F. (2017). Relationships between along-fault heterogeneous normal stress and fault slip patterns during the seismic cycle: Insights from a strike-slip fault laboratory model. *Earth and Planetary Science Letters*, *480*, 147-157. Retrieved from `https://www.sciencedirect.com/science/article/pii/S0012821X1730568X` doi: https://doi.org/10.1016/j.epsl.2017.10.009

Corbi, F., Sandri, L., Bedford, J., Funiciello, F., Brizzi, S., Rosenau, M., & Lallemand, S. (2019). Machine learning can predict the timing and size of analog earthquakes. *Geophysical Research Letters*, *46*(3), 1303-1311. doi: https://doi.org/10.1029/2018GL081251

Gao, K., Guyer, R., Rougier, E., & Johnson, P. (2020). Plate motion in sheared granular fault system. *Earth and Planetary Sci. Lett.*, *548*, 116481.

Gao, K., User, B., Rougier, E., Guyer, R., & Johnson, P. (2019). From stress chains to acoustic emission. *Physical. Rev. Lett.*, *123*, 048003.

Gao, K., User, B., Rougier, E., Guyer, R., Lei, Z., Knight, E., ... Carmelite, J. (2018). Modeling stick-slip behavior in sheared granules fault gouge using the fem/dem method. *JGR Solid Earth*, *123*(7), 5774-5792.

Holtzman, B. K., Paté, A., Paisley, J., Waldhauser, F., & Repetto, D. (2018). Machine learning reveals cyclic changes in seismic source spectra in geysers geothermal field [Journal Article]. *Science Advances*, *4*(5), eaao2929. doi: 10.1126/sciadv.aao2929

Hulbert, C., Rouet-Leduc, B., Johnson, P. A., Ren, C. X., Rivière, J., Bolton, D. C., & Marone, C. (2019). Similarity of fast and slow earthquakes illuminated by machine learning. *Nature Geoscience*, *12*(1), 69–74. doi: 10.1038/s41561-018-0272-8

Hulbert, C., Rouet-Leduc, B., Jolivet, R., & Johnson, P. A. (2020). An exponential build-up in seismic energy suggests a months-long nucleation of slow slip in Cascadia. *Nature Communications*, *11*(1), 4139. doi: 10.1038/s41467-020-17754-9

Jasperson, H., Bolton, D. C., Johnson, P., Guyer, R., Marone, C., & de Hoop, M. V. (2021). Attention network forecasts time-to-failure in laboratory shear experiments. *Journal of Geophysical Research: Solid Earth*, *126*(11), e2021JB022195. Retrieved from `https://agupubs.onlinelibrary.wiley.com/doi/abs/10.1029/2021JB022195` (e2021JB022195 2021JB022195) doi: https://doi.org/10.1029/2021JB022195

Johnson, C. W., Ben-Zion, Y., Meng, H., & Vernon, F. (2020). Identifying different classes of seismic noise signals using unsupervised learning [Journal Article]. *Geophysical Research Letters*, *47*(15), e2020GL088353. doi: https://doi.org/10.1029/2020GL088353

Johnson, C. W., & Johnson, P. (2023, 11). Seismic fingerprint predicts ground motions during the 2018 kilauea collapse sequence. doi: 10.21203/rs.3.rs-2500877/v1

Johnson, P. A., Rouet-Leduc, B., Pyrak-Nolte, L. J., Beroza, G. C., Marone, C. J., Hulbert, C., ... Reade, W. (2021). Laboratory earthquake forecasting: A machine learning competition. *Proceedings of the National Academy of Sciences*, *118*(5). doi: 10.1073/pnas.2011362118

Kong, Q., Trugman, D. T., Ross, Z. E., Bianco, M. J., Meade, B. J., & Gerstoft, P. (2018). Machine learning in seismology: Turning data into insights [Journal Article]. *Seismological Research Letters*. doi: 10.1785/0220180259

Latour, S., Voisin, C., Renard, F., Larose, E., Catheline, S., & Campillo, M. (2013). Effect of fault heterogeneity on rupture dynamics: An experimental approach using ultrafast ultrasonic imaging. *Journal of Geophysical Research: Solid Earth*, *118*(11), 5888-5902. Retrieved from `https://agupubs.onlinelibrary.wiley.com/doi/abs/10.1002/2013JB010231` doi: https://doi.org/10.1002/2013JB010231

Laurenti, L., Tinti, E., Galasso, F., Franco, L., & Marone, C. (2022). Deep learning for laboratory earthquake prediction and autoregressive forecasting of fault zone stress. *Earth and Planetary Science Letters*, *598*, 117825. Retrieved from `https://www.sciencedirect.com/science/article/pii/S0012821X22004617` doi: https://doi.org/10.1016/j.epsl.2022.117825

Lubbers, N., Bolton, D., Mohd-Yusof, J., Marone, C., Barros, K., & Johnson, P. (2018). Earthquake catalog-based machine learning identification of laboratory fault states and the effects of magnitude of completeness. *Geophysical Research Letters*, *45*. doi: 10.1029/2018GL079712

Marty, S., Schubnel, A., Bhat, H., Aubry, J., Fukuyama, E., Latour, S., ... Madariaga, R. (2023). Nucleation of laboratory earthquakes: Quantitative analysis and scalings. *Journal of Geophysical Research: Solid Earth*, *128*(3), e2022JB026294.

Mousavi, S. M., & Beroza, G. C. (2022). Deep-learning seismology. *Science*, *377*(6607), eabm4470. doi: doi:10.1126/science.abm4470

Mousavi, S. M., & Beroza, G. C. (2023). Machine learning in earthquake seismology [Journal Article]. *Annual Review of Earth and Planetary Sciences*, *51*(1), 105-

129. doi: 10.1146/annurev-earth-071822-100323

Rouet-Leduc, B., Hulbert, C., Bolton, D., Ren, C., Riviere, J., marone, C., ... Johnson, P. (2017). Estimating fault friction from seismic signals in the laboratory. *Geophys. Res. Lett..*, *45*, 1321-1329.

Rouet-Leduc, B., Hulbert, C., & Johnson, P. (2019a). Continuous chatter of cascadia subduction zone revealed by machine learning. *Nature Geoscience.*, *12*, 75-79.

Rouet-Leduc, B., Hulbert, C., & Johnson, P. A. (2019b). Continuous chatter of the Cascadia subduction zone revealed by machine learning. *Nature Geoscience*, *12*(1), 75–79. doi: 10.1038/s41561-018-0274-6

Selvadurai, P., & Glaser, S. (2016, 11). Asperity generation and its relationship to seismicity on a planar fault: a laboratory simulation. *Geophysical Journal International*, *208*(2), 1009-1025. Retrieved from `https://doi.org/10.1093/gji/ggw439` doi: 10.1093/gji/ggw439

Seydoux, L., Balestriero, R., Poli, P., Hoop, M. d., Campillo, M., & Baraniuk, R. (2020). Clustering earthquake signals and background noises in continuous seismic data with unsupervised deep learning [Journal Article]. *Nature Communications*, *11*(1), 3972. doi: 10.1038/s41467-020-17841-x

Shokouhi, P., Girkar, V., RiviÃšre, J., Shreedharan, S., Marone, C., Giles, C. L., & Kifer, D. (2021). Deep learning can predict laboratory quakes from active source seismic data. *Geophysical Research Letters*, *48*(12), e2021GL093187. Retrieved from `https://agupubs.onlinelibrary.wiley.com/doi/abs/10.1029/2021GL093187` (e2021GL093187 2021GL093187) doi: https://doi.org/10.1029/2021GL093187

Shreedharan, S., Bolton, D. C., RiviÃšre, J., & Marone, C. (2021). Machine learning predicts the timing and shear stress evolution of lab earthquakes using active seismic monitoring of fault zone processes. *Journal of Geophysical Research: Solid Earth*, *126*(7), e2020JB021588. doi: https://doi.org/10.1029/2020JB021588

Trugman, D., McBreaty, I., Bolton, D., Guyer, R., Marone, C., & Johnson, P. (2020). The patio-temporal evolution of granular microslip precursors to laboratory earthquakes. *Geophysical. Res. Lett.*, *47*, 2020GL088404.

Wang, K., Johnson, C. W., Bennett, K. C., & Johnson, P. A. (2021, 12). Predicting fault slip via transfer learning. *Nature Communications*, *12*. doi: 10.1038/s41467-021-27553-5

Wang, K., Johnson, C. W., Bennett, K. C., & Johnson, P. A. (2022). Predicting future laboratory fault friction through deep learning transformer models [Journal Article]. *Geophysical Research Letters*, *49*(19), e2022GL098233. doi: https://doi.org/10.1029/2022GL098233

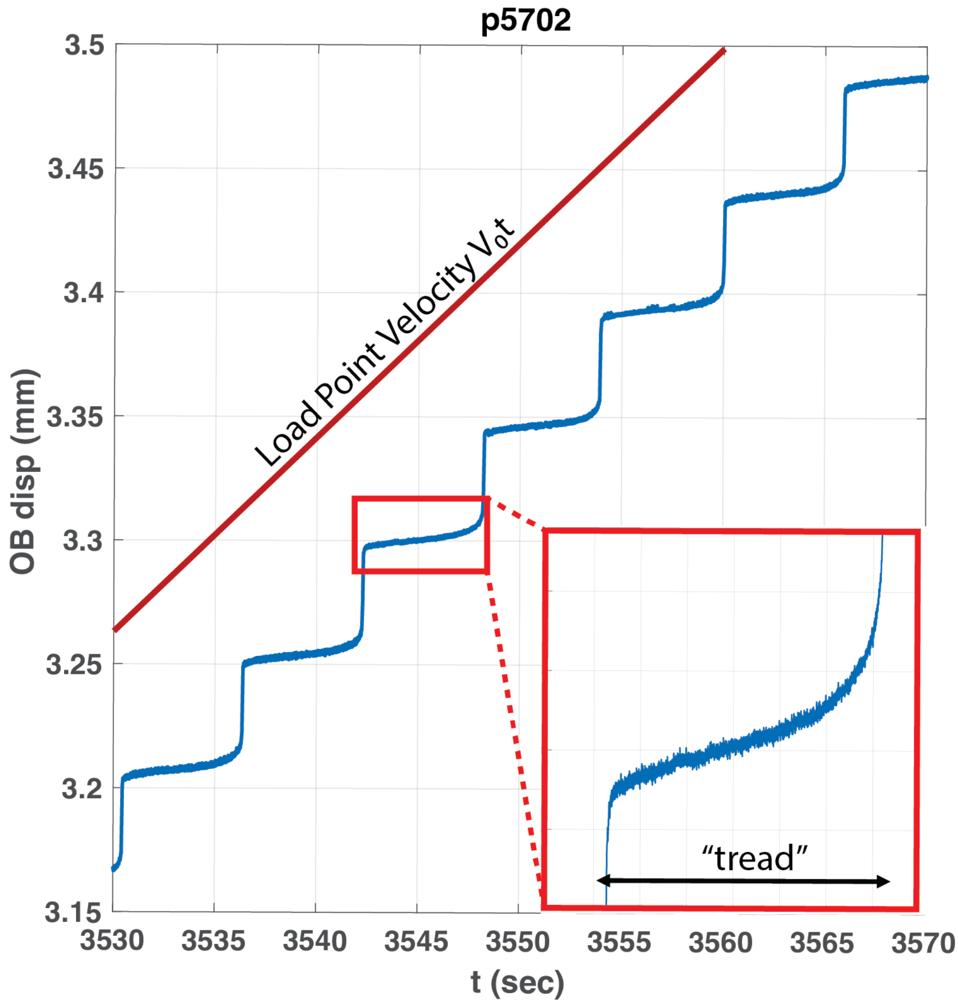

Figure 1. Shown in blue is the slider block on-board-displacement during the 6 MPa normal stress for the last six slip-cycles of the p5702 experiment. The red line shows the constant applied loading velocity of $V_0 = 10\ \mu m/sec$. The inset box is showing one "tread" as described in Section 2.2 Displacement for one loading cycle.

.

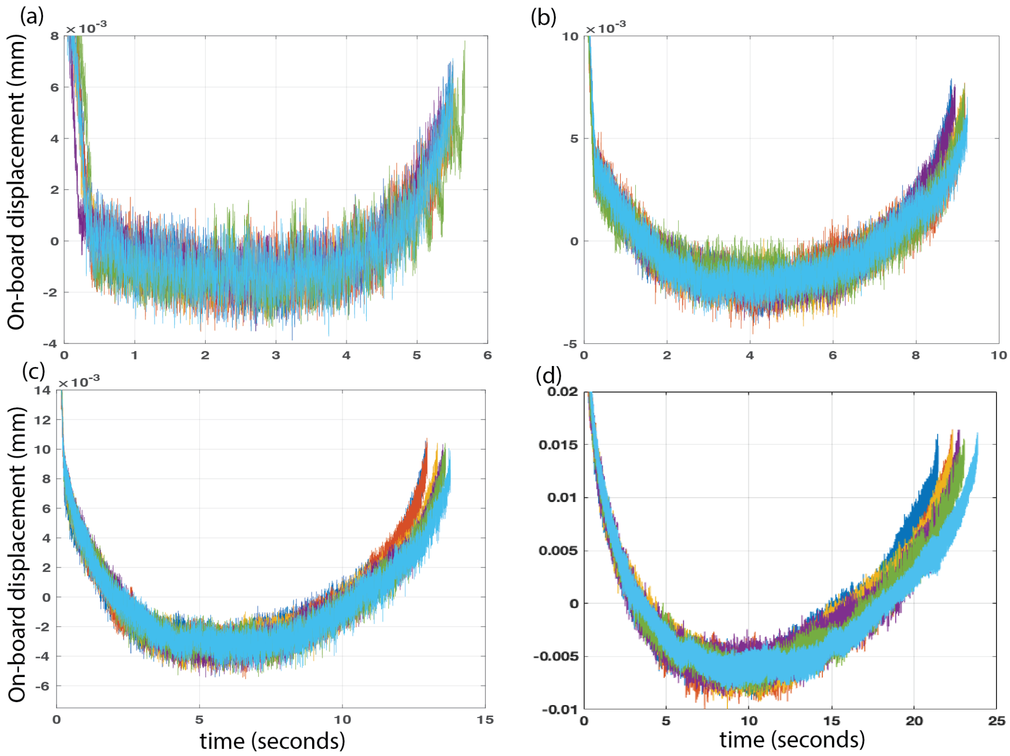

Figure 2. The six loading cycles on-board displacement stacked in time for the $N = 6, 9, 12, 15$ MPa experiments shown in (a), (b), (c), (d), respectively. Shown here is the on-board-displacement as measured from the shear stress using $a\tau = V_0 t - b - X_S$, with a and b found from the parameters characterizing the load cell. The on-board-displacement is directly measured in the experiment but there is increased variance in the direct measurement for $N = 12$ MPa and $N = 15$ MPa when compared to the shear stress.

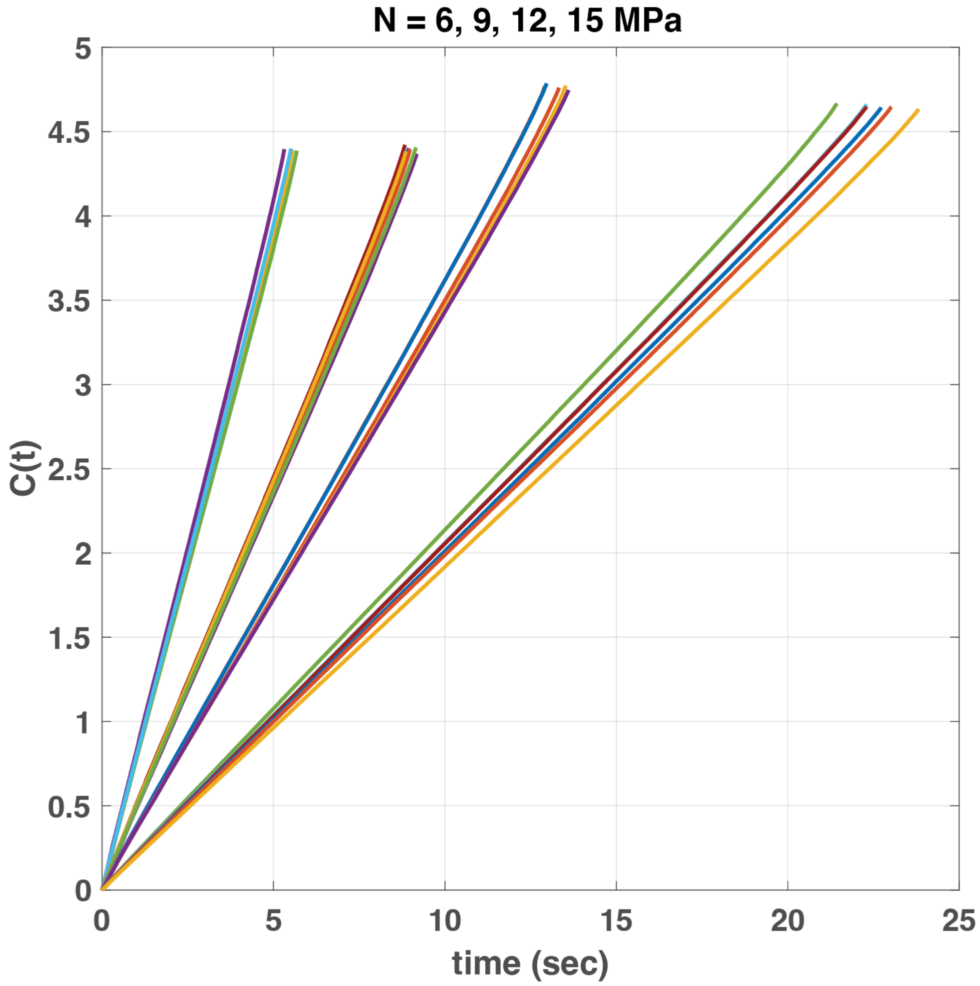

Figure 3. The integral $\mathcal{C}(t)$ from Equation 1 for the six "tread" values shown in groups from left to right for the increasing applied normal stress in the experiment.

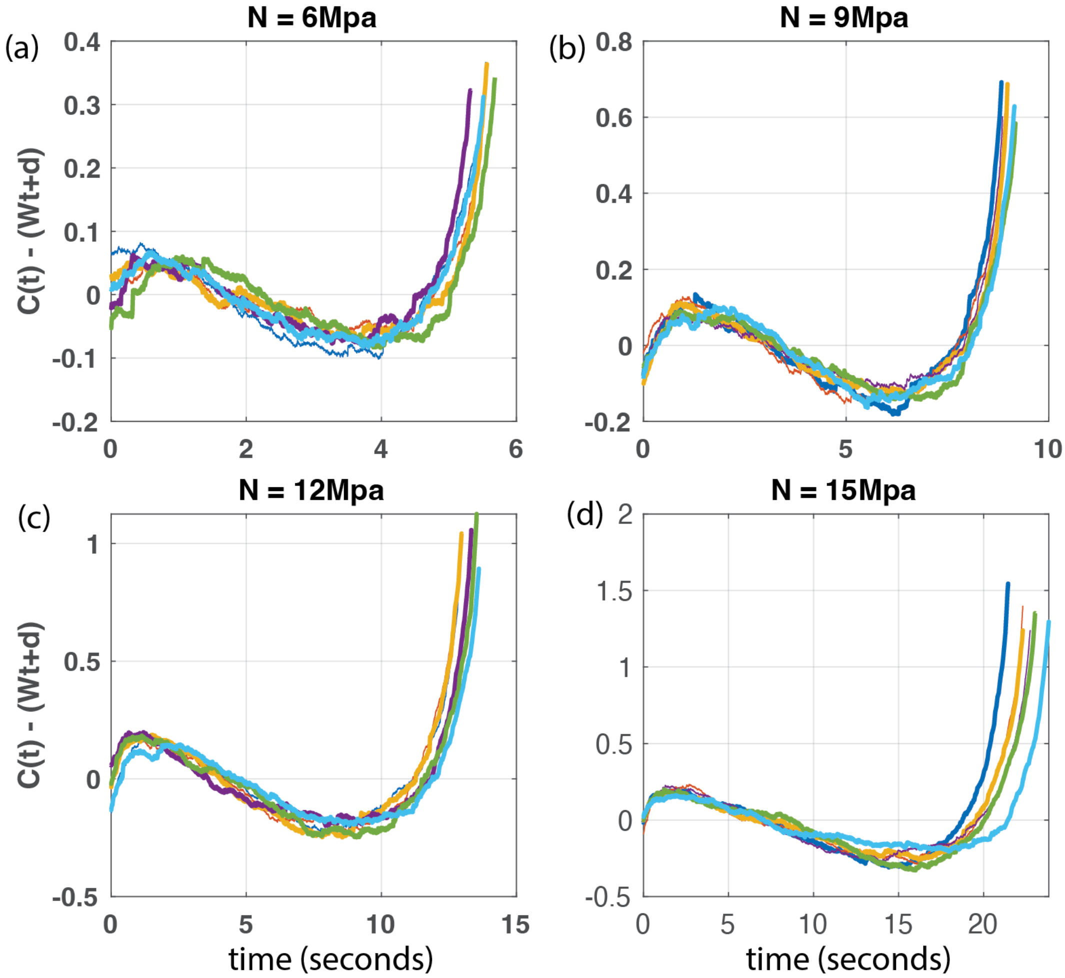

Figure 4. The residual values of $\mathcal{C}(t)$: $\mathcal{C}_a(t) = \mathcal{C}(t) - (Wt + d)$ for the six applied normal stresses in the experiment. Each "treads" during is shown in a different color for each experiment.